Available online at www.sciencedirect.com

ScienceDirect

Ceramics International 39 (2013) 9215–9221

CERAMICS INTERNATIONAL

www.elsevier.com/locate/ceramint

Ionic conductivity of apatite-type solid electrolyte ceramics $Ca_{2-x}Ba_xLa_4Bi_4(SiO_4)_6O_2$ ($0 \leq x \leq 2$)

M. Abbassi[a], R. Ternane[a,*], I. Sobrados[b], A. Madani[c], M. Trabelsi-Ayadi[a], J. Sanz[b]

[a]*Laboratoire d'Application de la Chimie aux Ressources et Substances Naturelles et à l'Environnement (LACReSNE), Université de Carthage, Faculté des Sciences de Bizerte, 7021 Zarzouna, Bizerte, Tunisia*

[b]*Instituto de Ciencia de Materiales de Madrid (ICMM), Consejo Superior de Investigaciónes Científicas (CSIC), Cantoblanco, 28049 Madrid, Spain*

[c]*Laboratoire de Physique des Matériaux, Université de Carthage, Faculté des Sciences de Bizerte, 7021 Zarzouna, Bizerte, Tunisia*

Received 26 February 2013; received in revised form 3 May 2013; accepted 7 May 2013
Available online 14 May 2013

Abstract

A complex impedance of oxyapatites $Ca_{2-x}Ba_xLa_4Bi_4(SiO_4)_6O_2$ ($0 \leq x \leq 2$) prepared by solid state reaction has been investigated. The formation of apatites has been checked by X-ray diffraction, FTIR, Raman and ^{29}Si MAS-NMR techniques. The electric impedance data indicate that relaxation phenomena are strongly dependent on temperature in the 923–1048 K range. The bulk resistance decreases with increasing temperature, showing a typical negative temperature coefficient of resistance (NTCR). ac-Conductivity measurements have been performed on a wide range of frequencies and temperatures. The complex modulus plots have confirmed the presence of bulk contributions. The complex impedance analysis suggests the presence of non-Debye relaxations that would be associated with correlation on ions motion.

Keywords: A. Powders: chemical preparation; C. Ionic conductivity; D. Apatite; E. Fuel cells

1. Introduction

At present, the finding of new solid electrolytes for Intermediate Temperature Solid Oxide Fuel Cells (IT-SOFCs) conditions efficient and cheap energy production. Among the most technologically promising ionic conducting electrolytes, ceramic samples with apatite-type structure fulfill most of the IT-SOFCs device requirements, working in the temperature range from 873 to 1073 K [1–11].

Oxyapatites, with general formula $Me_{10}(XO_4)_6O_2$ (space group $P6_3/m$), are based on isolated XO_4 tetrahedra that share oxygens with Me polyhedra to form a rigid network. In these compounds, O (5) oxide ions, occupying the center of one-dimensional channels running along the *c*-axis, are responsible of ionic conduction. Me cations are located on 7 and 9 coordinated sites, labeled respectively Me_I and Me_{II} sites. The apatite's structure can tolerate an appreciable number of structural defects, vacancies and interstitial atoms, varying the electrical properties appreciably with cation doping.

It should be pointed out that so far, there has hardly been extensive literature on apatites containing Bi^{3+}. Two leading syntheses are to be mentioned; one by Huang et al. [12] and the other by White et al. [13]. Both of them held the belief that due to the presence of $6s^2$ lone pair of electrons, Bi^{3+} substitution leads to a distortion in the Ca site, resulting in three different Ca sites, Ca(1), Ca(2) and Ca(3). This results in the loss of mirror plane and the space group thus changes from ideal $P6_3/m$ to $P6_3$. Similarly, the phosphate analogs $Ca_8Bi_2(PO_4)_6O_2$ and $Ca_8La_2(PO_4)_6O_2$ have been reported more recently [14].

In apatite-type silicates, Eu^{3+} luminescence has been used as a local structure probe in understanding the preferential occupancy of Bi^{3+} in the irregular hexacoordinated Ca_{II} site [15,16]. More recently, new bismuth calcium silicon oxide, $Ca_4Bi_{4.3}(SiO_4)(HSiO_4)_5O_{0.95}$, with an apatite structure has been synthesized and its structure has been refined [17].

*Corresponding author. Tel.: +216 98 90 19 16; fax: +216 72 59 05 66.
E-mail address: rternane@yahoo.fr (R. Ternane).

0272-8842/$ - see front matter © 2013 Elsevier Ltd and Techna Group S.r.l. All rights reserved.
http://dx.doi.org/10.1016/j.ceramint.2013.05.026

However, no systematic study has focused on the ionic conductivity in Bi^{3+} containing apatite-type silicates to our knowledge.

Complex impedance spectroscopy is a well-established method to investigate electrical properties of materials. This technique offers enormous possibilities to investigate the electrical and electrochemical properties of materials. Thanks to this technique, the study of relaxation phenomena, and the resolution of bulk, grain boundaries and electrode–electrolyte interface contributions are often produced.

In this work, $Ca_{2-x}Ba_xLa_4Bi_4(SiO_4)_6O_2$ ($0 \leq x \leq 2$) oxyapatites have been prepared by solid state reaction as a first step. Then, the structural characterization of prepared materials has been performed with XRD, FTIR, Raman and MAS-NMR techniques. Finally, oxygen conductivity and electrical properties of these oxyapatites have been investigated by complex impedance spectroscopy.

2. Experimental

2.1. Synthesis

The oxyapatites $Ca_{2-x}Ba_xLa_4Bi_4(SiO_4)_6O_2$ ($0 \leq x \leq 2$) have been prepared by solid state reaction, using high purity SiO_2 (99.99%), $CaCO_3$ (99%), La_2O_3 (99%), $BaCO_3$ (99.9%) and Bi_2O_3 (99%) powders. Stoichiometric amounts of reactants have been ground and heated in covered platinum crucibles at 1173 K for 24 h and at 1523 K for 24 h.

2.2. Experimental techniques

X-ray diffraction (XRD) patterns have been recorded with a Bruker D8-advance diffractometer using Cu Kα radiation ($\lambda = 1.5406$ Å). X-ray diffraction data have been collected over the 10°–60° 2θ range with a 0.02° step and at regular intervals of 12 s. The crystalline phases have been identified using the International Centre for Diffraction Data (ICDD) powder diffraction files.

Fourier transformed infrared (FTIR) spectra have been obtained with a Bruker spectrometer, in the 4000–400 cm^{-1} range, using the KBr pellet technique. Raman spectra have been recorded at room temperature in the spectral range 100–1200 cm^{-1} in a Dilor XY spectrometer equipped with a CCD detector and a Spectra Physics Ar laser (excitation at 514.5 nm).

The ^{29}Si MAS-NMR spectra have been recorded at 79.49 MHz, using a Bruker MSL400 spectrometer (9.4 T). The sample has been rotated at 10 kHz around an axis inclined 54.44° with respect to the external magnetic field (MAS technique). NMR signals have been recorded after π/2 radio-frequency pulse (5 μs) irradiation. Accumulations have reached 100, each separated from its successor by 20 s. To improve signal/noise ratios, a 100 kHz filter has been used.

Electrical conductivity measurements of apatite materials have been performed using an automatically controlled HP4192A analyzer working at 120 frequencies, log-scaled between 5 Hz and 13 MHz. In electrical measurements, a sinusoidal signal of 50 mV has been used. High temperature measurements have been performed between 748 and 1073 K under air atmosphere. Powders have been pressed under 5 t cm^{-2} and sintered at 1523 K. Electrodes have been prepared by painting Pt paste on both sides of the sintered pellet surfaces, which have been then heated at 1028 K to ensure good electrical contacts. Conductivity values have been estimated with the relation

$$\sigma = \frac{l}{RS} \quad (1)$$

where R is the resistance deduced from impedance diagrams and S and l are the area and the thickness of pellets, respectively.

3. Results and discussion

3.1. X-ray diffraction

Powder XRD patterns of prepared $Ca_{2-x}Ba_xLa_4Bi_4(SiO_4)_6O_2$ compounds correspond to well crystallized phases. XRD patterns have been fitted with the hexagonal unit cell (S.G. $P6_3$ (173)). XRD patterns have showed that all prepared samples are single phases displaying the apatite structure. No peaks of additional phases have been detected. Crystal data deduced from XRD analysis are given in Table 1.

As shown in Fig. 1 and Table 1, lattice parameters are influenced by the Ba content. The a and c parameters and unit cell volume (V) increase with Ba^{2+} incorporation to the apatite ($r^{2+}_{Ba} = 1.38$ Å, $r^{2+}_{Ca} = 1.06$ Å) [18]. The evolution of a and c unit cell parameters follows a linear dependence, indicating the occurrence of a continuous solid solution in oxyapatites network (Vegard's law).

Table 1
Unit cell parameters of $Ca_{2-x}Ba_xLa_4Bi_4(SiO_4)_6O_2$ oxyapatites.

Ba content (x)	0	0.5	1	1.5	2
a (Å)	9.635	9.648	9.673	9.726	9.779
c (Å)	7.125	7.143	7.172	7.237	7.323
V (Å^3)	384.056	386.111	389.685	397.494	406.593
Crystal system	Hexagonal				
Space group	$P6_3$				

3.2. Vibrational infrared spectra

The assignments of infrared (IR) bands of pure oxyapatites have been performed according to published literature [16,19,20]. IR spectra displayed absorption bands between 966 and 870 cm^{-1} (symmetric and antisymmetric stretching bands) and relatively sharp bands between 547 and 450 cm^{-1} (symmetric and antisymmetric bending vibrations) due to isolated SiO_4 tetrahedra. These bands confirm the presence of orthosilicate groups in prepared materials. The broadness observed in absorption bands can be ascribed to minor distortions of SiO_4 groups from the ideal T_d symmetry [16]. The band assignment is given in Table 2.

One can note the absence of the characteristic bands of OH^- groups located at 3572 cm^{-1} (ν_S: stretching mode) and at 630 cm^{-1} (ν_L: librational mode) in IR spectra of oxyapatites. The absence of bands at 1118 cm^{-1} and 846 cm^{-1}, characteristic of Si–O–Si bonds, confirms the absence of secondary phases with disilicate structure [21]. These results confirm the purity of the investigated samples.

3.3. Vibrational Raman spectra

Fig. 2 shows the Raman spectra for the $Ca_{2-x}Ba_xLa_4Bi_4(SiO_4)_6O_2$ oxyapatites in the 100–1200 cm^{-1} range. The observed major band positions can be assigned to their corresponding modes based on the related silicate apatite samples in literature [20,22–26]. The band positions are summarized in Table 2.

The presence of isolated SiO_4 groups is revealed by the significant intensity of 842–851 and 900 cm^{-1} bands, associated with symmetric (ν_s) and asymmetric (ν_{as}) stretching modes, respectively. The bands appearing in ranges 364–391 cm^{-1} and 514–516 cm^{-1} are assigned to the symmetric (δ_s) and asymmetric (δ_{as}) bending modes of SiO_4, respectively.

The increase in the Ba^{2+} content induces small shifts of Raman bands towards lower frequencies.

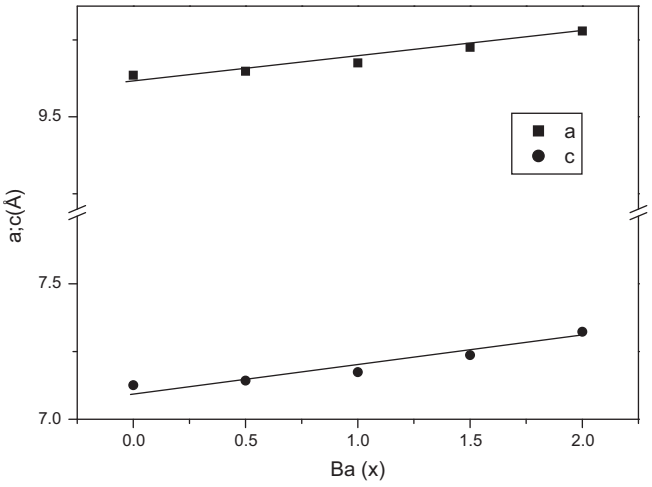

Fig. 1. Variation of a and c unit cell parameters with the Ba content (x) in $Ca_{2x}Ba_xLa_4Bi_4(SiO_4)_6O_2$ oxyapatites.

3.4. NMR spectroscopy

^{29}Si MAS-NMR spectra of $Ca_{2-x}Ba_xLa_4Bi_4(SiO_4)_6O_2$ oxyapatites are given in Fig. 3. The corresponding data are summarized in Table 3. NMR data are consistent with structure of apatites, where isolated tetrahedral $[SiO_4]^{4-}$ units are present [22,27–29]. In apatites, only one tetrahedral site is present. Based on structural features of apatites' structures, distortions of the SiO_4 group are always small.

When barium ions are incorporated into the structure, a systematic shift towards low frequencies and the broadening of central components are often observed. The presence of more

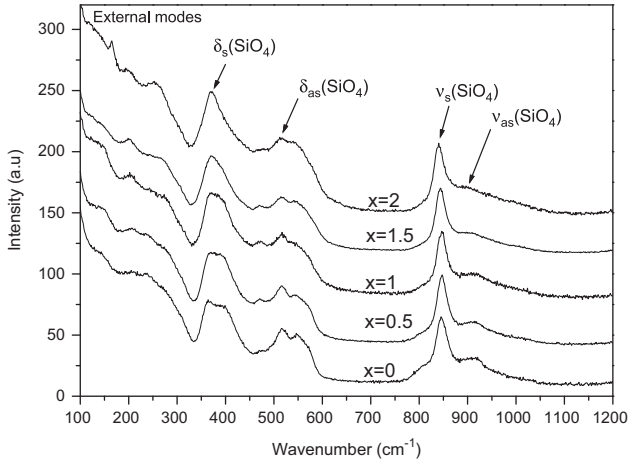

Fig. 2. Raman spectra of $Ca_{2-x}Ba_xLa_4Bi_4(SiO_4)_6O_2$ oxyapatites.

Table 2
Assignments (cm^{-1}) of FT-IR and Raman spectra of $Ca_{2-x}Ba_xLa_4Bi_4(SiO_4)_6O_2$ oxyapatites.

	Infrared spectroscopy				Raman spectroscopy			
Compound	ν_s	δ_s	ν_{as}	δ_{as}	ν_s	δ_s	ν_{as}	δ_{as}
$Ca_2La_4Bi_4(SiO_4)_6O_2$	870	–	937–966	547–490	846	397–364	920	516
$Ca_{1.5}Ba_{0.5}La_4Bi_4(SiO_4)_6O_2$	870	–	933	547–490	846	393–367	920	516
Ca $BaLa_4Bi_4(SiO_4)_6O_2$	870	–	928	547–490	846	393–367	920	516
$Ca_{0.5}Ba_{1.5}La_4Bi_4(SiO_4)_6O_2$	870	–	916	542–489	843	371	910	516
$Ba_2La_4Bi_4(SiO_4)_6O_2$	870	450	910	536–489	840	370	903	514

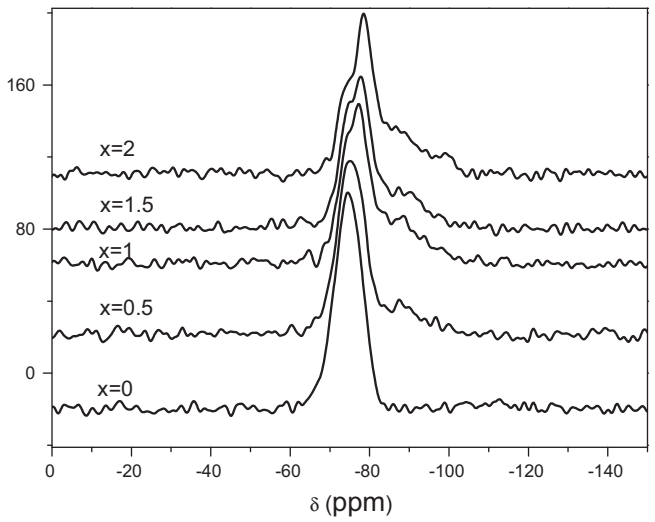

Fig. 3. ^{29}Si MAS-NMR spectra of $Ca_{2-x}Ba_xLa_4Bi_4(SiO_4)_6O_2$ oxyapatites.

Table 3
^{29}Si MAS-NMR chemical shifts in $Ca_{2-x}Ba_xLa_4Bi_4(SiO_4)_6O_2$ oxyapatites.

Ba content (x)	δ (ppm)			
0	−74.7			
0.5	−74.7	−77.9	−87.2	−96.5
1	−74.7	−77.2	−87.2	−98.3
1.5	−74.7	−77.4	−87.2	−97.8
2	−74.7	−78.3	−86.6	−99.5

than one peak for some compositions indicates that not all $[SiO_4]^{4-}$ units are chemically equivalent.

Take into account that structural refinements only indicate the presence of one structural site for Si atoms, different observed components should be ascribed to different chemical environments around Si tetrahedra. The existence of a higher amount of polarizing (La^{3+} or Bi^{3+}) cations around Si tetrahedra, that share oxygen with Si atoms, makes the position of Si components shift to more negative values.

Different components detected in ^{29}Si MAS-NMR spectra are ascribed to Si environments with different amounts of divalent Ca and Ba in Me_I or Me_{II} sites. The structural analysis of oxyapatites shows that Si tetrahedra share oxygen atoms with four Me_{II} and three Me_I cations. Take into account the average charge provided by divalent cations at Me sites, the most probable cationic environments around tetrahedra must be $(Ca,Ba)_n(La,Bi)_{7-n}$, with n=1 and 2. Based on this estimation, bands centered at −95 and −74/−78 ppm are ascribed to $(Ca,Ba)_1(La,Bi)_6$ and $(Ca,Ba)_2(La,Bi)_5$ environments, respectively.

The analysis of spectra suggests that the intensity of the −92 ppm component increases at intermediate Ca,Ba compositions and disappears at two end members of the series. These observations suggest that the substitution of Ca by Ba cations increases considerably the cation disordering at intermediate compositions. This point would be discussed later on when variations on oxygen conductivity will be related to cation disordering in oxyapatites.

3.5. Oxide ion conductivity

3.5.1. Complex electrical impedance analysis

Fig. 4 shows typical complex impedance spectra (Nyquist plots) of $Ba_2La_4Bi_4(SiO_4)_6O_2$ oxyapatite over a wide range of temperatures. The impedance spectra of the samples are characterized by the appearance of a single semicircular arc. This peak is attributed to the presence of single electrical relaxation phenomena in materials under investigation [30].

The intercept of semicircular arc with the real axis gives an estimate of the sample resistance. The absence of a second semicircle in complex impedance plots suggests the dominance of bulk contributions in the oxyapatites. Impedance spectra were fitted satisfactorily with a parallel R-CPE circuit model. As temperature increases, the radius of the arc corresponding to the bulk resistance of samples decreases, indicating the existence of activated conduction mechanisms. The observed behavior of materials is analogous to the negative temperature coefficient of resistance (NTCR) reported in semiconductors. In all cases, resistance of bulk conductivity increases with the rise in temperature.

3.5.2. ac-Conductivity

ac Conductivity measurement is an important tool for studying the ionic transport properties of materials. When an ac electric current passes through the solid electrolyte, processes like ion motion through bulk of the electrolyte, charge transfer across the electrode–electrolyte interface, etc., take place.

Fig. 5(a) shows the variation of the ac conductivity (σ_{ac}) with frequency at different temperatures of $Ba_2La_4Bi_4(SiO_4)_6O_2$. It is clearly observed that high and low frequency regions can be separated by a change in slope for each temperature. The frequency at which the slope of conductivity changes is known as the "hopping frequency ω_p." It is important to note that the values of hopping frequencies are observed to go up with the increase in temperature. Fig. 5(a) shows that σ_{ac} decreases with decreasing frequency and

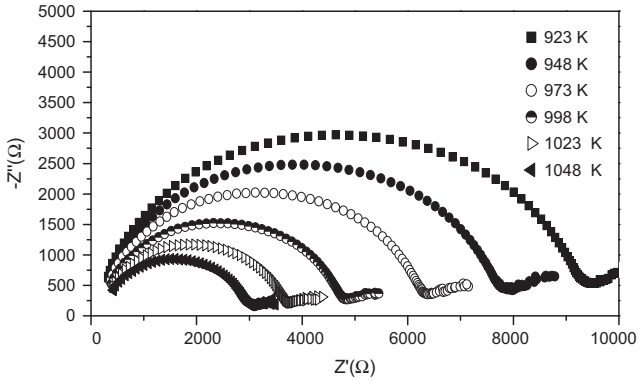

Fig. 4. Nyquist diagrams ($-Z''$ versus Z') of $Ba_2La_4Bi_4(SiO_4)_6O_2$ oxyapatite.

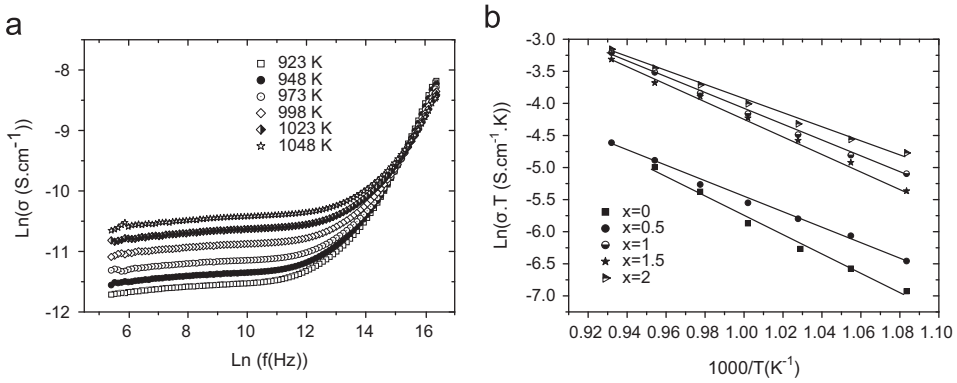

Fig. 5. (a) Frequency dependence of ac conductivity at different temperatures of $Ba_2La_4Bi_4(SiO_4)_6O_2$ oxyapatite. (b) Arrhenius plots of $Ca_{2-x}Ba_xLa_4Bi_4(SiO_4)_6O_2$ oxyapatites.

becomes independent of frequency after a certain value. At higher frequencies, the values of ac electrical conductivity (σ_{ac}) become closer, and are temperature-independent. The frequency dependence of σ_{ac} can be described by the Jonscher universal power law: $\sigma_{ac}(\omega) = \sigma_{dc}[1 + (\omega/\omega_p)^n]$ [31], where (σ_{dc}) is the dc conductivity obtained from the extrapolation to zero frequency of the Ln σ_{ac} versus Ln f curves, ω_p is the hopping frequency of the charge carriers, where $\sigma_{ac}(\omega) = 2\sigma_{dc}(0)$, and n is the frequency exponent, describing ion–ion interactions in hopping process; i.e., the exponent n would be 0 for random ion hopping (absence of interactions) whereas it tends to 1 for fully correlated ion motions [32,33].

The exponent n values are calculated by fitting the frequency dependence of the isothermal conductivity data to the above mentioned extended Jonscher-type expression (Fig. 5a). The variation of n as a function of temperature can directly be related to the existence of a range of relaxation processes and ion diffusion mechanism in the network of the $Ca_{2-x}Ba_xLa_4Bi_4(SiO_4)_6O_2$ oxyapatites. Hence, from impedance and power law plots, it is observed that the frequency at which the Z'' attains a maximum and the frequency ω_p at which relaxation effects begin to shift to higher frequencies with increase in temperature.

Fig. 5(b) shows the Ln(σT) versus 1000/T plot of the $Ca_{2-x}Ba_xLa_4Bi_4(SiO_4)_6O_2$ oxyapatites. It is clear that from the slope plot that activation energy values, $E_{a\sigma}$, can be calculated. The results listed in Table 4 show that, in most cases, single Arrhenius plots are obtained. Fig. 6(a and b) shows the variation in the bulk conductivity and the activation energy as a function of the Ba-content. A maximum conductivity appears for the $x=2$ composition. This maximum corresponds to the lowest activation energy.

The variation of the conductivity may be attributed to entropy and enthalpy terms of the equation

$$\sigma \times T = A \exp\left(\frac{\Delta S}{K}\right) \exp\left(\frac{\Delta H}{KT}\right) \quad (2)$$

Fig. 6(a) shows the conductivities of $Ca_{2-x}Ba_xLa_4Bi_4(SiO_4)_6O_2$ ($0 \le x \le 2$) at 923, 973 and 1023 K. At each temperature, an increase of conductivity is observed. The conductivity values at 973 K and the activation energies for different compositions are reported in Table 4. We may notice first the low conductivity of the undoped apatite and the significant increase of conductivity with Ba^{2+} doping on the Ca^{2+} site. The best conductivity and the lowest activation energy are observed for the $x=2$ composition ($1.37\ 10^{-5}$ S cm^{-1} at 973 K and $E_{a\sigma} = 0.95$ eV).

In stoichiometric oxyapatites, conduction mechanisms are probably related to the translational hopping of O^{2-} ions along the c-axis, from ordinary lattice sites to interstitial sites, and back again to structural sites. In general, O^{2-} ions must be able to move to other positions by the formation of thermally actived Schottky defects with higher activation energies.

Fig. 7(a) shows the dependence of the imaginary part of impedance (Z'') of $Ba_2La_4Bi_4(SiO_4)_6O_2$ oxyapatite on frequency at different temperatures. This peak shifts to higher frequencies when temperature increases. It indicates a thermally activated dielectric relaxation process and shows a progressive decrease in the bulk resistance when temperature increases. These peaks have not been detected at low temperatures, suggesting the presence of weak current dissipations in the material or relaxation frequency beyond the measurement window. The significant broadening of peaks with rising temperature suggests the presence of a temperature dependent relaxation process. The asymmetric broadening of peaks suggests the presence of some electrical processes in the materials that spread relaxation times. This behavior is again due to the presence of space charge polarizations at lower frequencies disappearing at higher frequencies [31,34].

Indeed, at higher temperatures, the peak height representing the relaxation shows a progressive increment with Ba content.

The impedance data are used to evaluate the relaxation time (τ) of the electrical phenomena in the material using the relation

$$\tau = \frac{1}{\omega_{max}} = \frac{1}{2\Pi f_{max}} = RC \quad (3)$$

where f_{max} is the relaxation frequency. The variation of τ with temperature is shown in Fig. 7(b). These plots show a steady increase in the relaxation time with rising temperature. This result suggests the presence of temperature-dependent electrical relaxation phenomena in the material, possibly due to the migration of species/defects. All the curves were found to follow the Arrehenius relation,

$$\tau = \tau_0 \exp\left(\frac{E_{a\tau}}{KT}\right) \quad (4)$$

Table 4
Summary of conductivity data of $Ca_{2-x}Ba_xLa_4Bi_4(SiO_4)_6O_2$ oxyapatites.

Ba content (x)	$\sigma_{973\ K}$ (S cm^{-1})	$\tau_{973\ K}$ (s)	$E_{a\sigma}$ (eV)	$E_{a\tau}$ (eV)
0	1.79×10^{-6}	2.52×10^{-6}	1.19	1.17
0.5	3.11×10^{-6}	1.72×10^{-6}	1.02	1.04
1	1.15×10^{-5}	3.17×10^{-7}	1.08	1.06
1.5	1.07×10^{-5}	3.17×10^{-7}	1.13	1.15
2	1.37×10^{-5}	1.59×10^{-7}	0.95	0.90

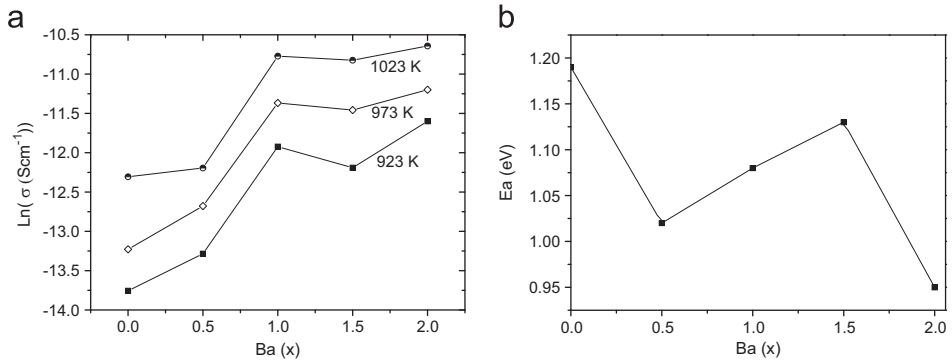

Fig. 6. (a) Variation of the conductivity as a function of Ba content (x). (b) Variation of the activation energy as a function of Ba content (x) in $Ca_{2-x}Ba_xLa_4Bi_4(SiO_4)_6O_2$ oxyapatites.

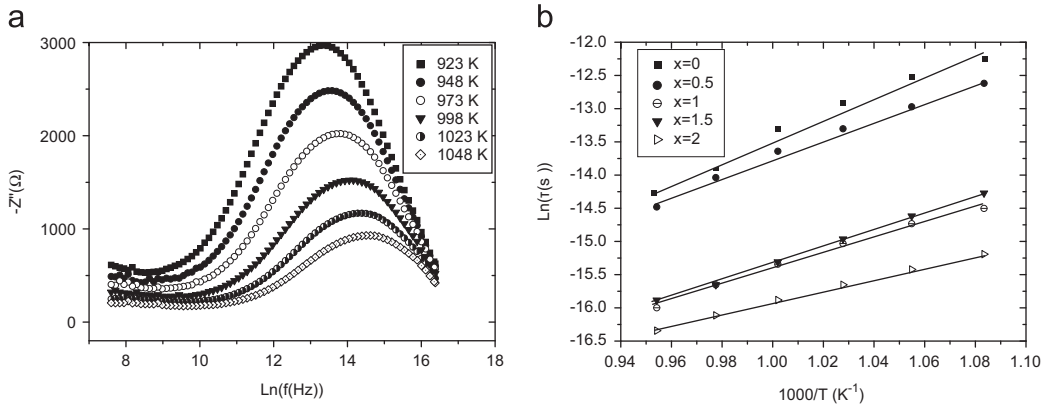

Fig. 7. (a) Frequency dependence of the imaginary part (Z'') of $Ba_2La_4Bi_4(SiO_4)_6O_2$ oxyapatite. (b) Dependence of the relaxation time with inverse of temperature in $Ca_{2-x}Ba_xLa_4Bi_4(SiO_4)_6O_2$ oxyapatites.

where τ_0 is a pre-exponential factor, $E_{a\tau}$ is the activation energy, k is the Boltzmaan constant and T is the absolute temperature. Activation energies ($E_{a\tau}$) estimated from the slope of the log (τ) against 1000/T curve are given in Table 4.

4. Conclusion

Oxyapatites $Ca_{2-x}Ba_xLa_4Bi_4(SiO_4)_6O_2$ ($0 \le x \le 2$) have been synthesized by the solid state reaction. XRD has confirmed the formation of single apatite phases. FTIR, Raman and ^{29}Si MAS-NMR spectroscopies have confirmed the formation of isolated SiO_4 groups in analyzed samples.

Complex impedance spectroscopy, which has been used to investigate the electrical behavior of $Ca_{2-x}Ba_xLa_4Bi_4(SiO_4)_6O_2$ ($0 \le x \le 2$) compounds, has shown that complex impedance spectra inform about the possible contribution of bulk contributions and temperature-dependent relaxation phenomena.

From the impedance spectroscopic plots, deviations from Debye relaxations are detected in analyzed apatites. The relaxation frequencies shift to a higher frequency side with increasing temperature. The frequency dependence of ac conductivity data follows the 'universal' power Jonscher's law in analyzed apatites.

Acknowledgments

The authors would like to thank Gerard Panczer, Professor at the University Claude Bernard Lyon I, for his invaluable assistance in Raman spectra acquisition and the language expert Besma Wachem for proofreading the manuscript.

References

[1] P. Berastegui, S. Hull, F.J.G. Garcia, J. Grins, A structural investigation of $La_2(GeO_4)O$ and alkaline-earth-doped $La_{9.33}(GeO_4)_6O_2$, Journal of Solid State Chemistry 168 (2002) 294–305.

[2] E.J. Abram, D.C. Sinclair, A.R. West, A novel enhancement of ionic conductivity in the cation-deficient apatite $La_{9.33}(SiO_4)_6O_2$, Journal of Materials Chemistry 11 (2001) 1978–1979.

[3] H. Arikawa, H. Nishiguchi, T. Ishihara, Y. Takita, Oxide ion conductivity in Sr-doped $La_{10}Ge_6O_{26}$ apatite oxide, Solid State Ionics 136 (2000) 31–37.

[4] S. Nakayama, M. Sakamoto, M. Higuchi, K. Kodaira, M. Sato, S. Kakita, T. Suzuki, K. Itoh, Oxide ionic conductivity of apatite type $Nd_{9.33}(SiO_4)_6O_2$ single crystal, Journal of European Ceramic Society 19 (1999) 507–510.

[5] A.L. Shaula, V.V. Kharton, F.M.B. Marques, Ionic and electronic conductivities, stability and thermal expansion of $La_{10-x}(Si,Al)_6O_{26\pm\delta}$ solid electrolytes, Solid State Ionics 177 (2006) 1725–1728.

[6] A.L. Shaula, V.V. Kharton, J.C Waerenborgh, D.R. Rojas, F.M.B. Marques, Oxygen ionic and electronic transport in apatite ceramics, Journal of European Ceramic Society 25 (2005) 2583–2586.

[7] P.R. Slater, J.E.H. Sansom, J.R. Tolchard, Development of apatite-type oxide ion conductors, The Chemical Record 4 (2004) 373–384.

[8] A Orera, D Headspith, D.C Apperley, M.G Francesconi, P.R. Slater, Formation of apatite oxynitrides by the reaction between apatite-type oxide ion conductors $La_{8+x}Sr_{2-x}(Si/Ge)_6O_{26+x/2}$, and ammonia, Journal of Solid State Chemistry 182 (2009) 3294–3298.

[9] A. Jones, P.R. Slater, M.S. Islam, Local defect structures and ion transport mechanisms in the oxygen-excess apatite $La_{9.67}(SiO_4)_6O_{2.5}$, Chemistry of Materials 20 (2008) 5055–5060.

[10] E. Jothinathan, K. Vanmeensel, J. Vleugels, O. Van der Biest, Synthesis of nano-crystalline apatite type electrolyte powders for solid oxide fuel cells, Journal of European Ceramic Society 30 (2010) 1699–1706.

[11] N. Nallamuthu, I. Prakash, N. Satyanarayana, M. Venkateswarlu, Electrical conductivity studies of nanocrystalline lanthanum silicate synthesized by sol–gel route, Journal of Alloys and Compounds 509 (2011) 1138–1145.

[12] J. Huang, A.W. Sleight, The apatite without an inversion center in a new bismuth calcium vanadium oxide: $BiCa_4V_3O_{13}$, Journal of Solid State Chemistry 104 (1993) 52–58.

[13] T.J. White, D. ZhiLi, Structural derivation and crystal chemistry of apatites, Acta Crystallographica B 59 (2003) 1–16.

[14] G. Buvaneswari, U.V. Varadaraju, Synthesis and characterization of new apatite-related phosphates, Journal of Solid State Chemistry 149 (2000) 133–136.

[15] N. Lakshminarasimhan, U.V. Varadaraju, Eu^{3+} luminescence: a structural probe in $BiCa_4(PO_4)_3O$, an apatite related phosphate, Journal of Solid State Chemistry 177 (2004) 3536–3544.

[16] N. Lakshminarasimhan, U.V. Varadaraju, Synthesis and Eu^{3+} luminescence in new oxysilicates, $ALa_3Bi(SiO_4)_3O$ and $ALa_2Bi_2(SiO_4)_3O$ [A=Ca, Sr and Ba] with apatite-related structure, Journal of Solid State Chemistry 178 (2005) 3284–3292.

[17] V. Uvarov, S. Shenawi-Khalil, I. Popov, New bismuth calcium oxysilicate: synthesis and structure characterization, Journal of Solid State Chemistry 183 (2010) 1484–1489.

[18] R.D Shannon, Revised effective ionic radii and systematic studies of interatomic distances in halides and chalcogenides, Acta Crystallographica 32 (1976) 751–767.

[19] K. Boughzala, E. Ben Salem, A. Ben Chrifa, E. Gaudin, K. Bouzouita, Synthesis and characterization of strontium–lanthanum apatites, Materials Research Bulletin 42 (2007) 1221–1229.

[20] R. El Ouenzerfi, C. Goutaudier, G. Panczer, B. Moine, M.T. Cohen-Adad, M. Trabelsi-Ayedi, N. Kbir-Ariguib, Investigation of the CaO–La_2O_3–SiO_2–P_2O_5 quaternary diagram. Synthesis, existence domain, and characterization of apatitic phosphosilicates, Solid State Ionics 156 (2003) 209–222.

[21] C. Peng, G. Li, X. Kang, C. Li, J. Lin, The fabrication of one-dimensional $Ca_4Y_6(SiO_4)_6O$: Ln^{3+} (Ln=Eu, Tb) phosphors by electrospinning method and their luminescence properties, Journal of Colloid and Interface Science 355 (2011) 89–95.

[22] S.H. Jo, P. Muralidharan, D.K. Kim, Raman and ^{29}Si NMR spectroscopic characterization of lanthanum silicate electrolytes: Emphasis on sintering temperature to enhance the oxide–ion conductivity, Electrochimica Acta 54 (2009) 7495–7501.

[23] R.E. Rodriguez, A.F. Fuentes, M. Maczka, J. Hanuza, K. Boulahya, U. Amador, Structural, microstructural and vibrational characterization of apatite-type lanthanum silicates prepared by mechanical milling, Journal of Solid State Chemistry 179 (2006) 522–531.

[24] G. Lucazeau, N. Sergent, T. Pagnier, A. Shaula, V. Kharton, F.M.B. Marques, Raman spectra of apatites: $La_{10-x}Si_{6-y}(Al,Fe)_yO_{26\pm\delta}$, Journal of Raman Specroscopy 38 (2007) 21–33.

[25] A. Orera, E. Kendrick, D.C. Apperley, V.M. Orera, P.R Slater, Effect of oxygen content on the ^{29}Si NMR, Raman spectra and oxide ion conductivity of the apatite series, $La_{8+x}Sr_{2-x}(SiO_4)_6O_{2+x/2}$, Dalton Transactions 39 (2008) 5296–5301.

[26] L. Zhang, H. Quan He, H. Wu, C. Li, S.P. Jiang, Synthesis and characterization of doped $La_9ASi_6O_{26.5}$ (A=Ca, Sr, Ba) oxyapatite electrolyte by a water-based gel-casting route, International Journal of Hydrogen Energy 36 (2011) 6862–6874.

[27] J.E.H. Sansom, J.R. Tolchard, M.S. Islam, D. Apperley, P.R. Slater, Solid state ^{29}Si NMR studies of apatite-type oxide ion conductors, Journal of Solid State Chemistry 16 (2006) 1410–1413.

[28] K. Boughzala, S. Naser, E. Ben Salem, F. Kooli, K. Bouzouita, Structural and spectroscopic investigation of lanthanum-substituted strontium-oxybritholites, Journal of the Chemical Society 121 (2009) 283–291.

[29] K. Boughzala, E. Ben Salem, F. Kooli, P. Gravereau, K. Bouzouita, Spectroscopic studies and Rietveld refinement of stronsium-brithoites, Journal of Rare Earths 26 (2008) 483–489.

[30] A. Molak, M. Paluch, S. Pawlus, J. Klimontko, Z. Ujma, I. Gruszka, Electric modulus approach to the analysis of electric relaxation in highly conducting $(Na_{0.75}Bi_{0.25})(Mn_{0.25}Nb_{0.75})O_3$ ceramics, Journal of Physics D: Applied Physics 38 (2005) 1450–1460.

[31] A.K. Jonscher, The universal dielectric response, Nature 267 (1977) 673–679.

[32] K. Funke, Jump relaxtion model and coupling model-a comparison, Journal of Non-Crystalline Solids 1215 (1994) 172–174.

[33] K.L. Ngai, K.Y. Tsang, Similarity of relaxation in supercooled liquids and interacting arrays of oscillators, Physical Review E 60 (1999) 4511–4517.

[34] R. Ranjan, R. Kumar, N. Kumar, B. Behera, R.N.P. Choudhary, Impedance and electric modulus analysis of Sm-modified Pb$(Zr_{0.55}Ti_{0.45})_{1-x/4}O_3$ ceramics, Journal of Alloys and Compounds 509 (2011) 6388–6394.